Angle-Resolved Direct Emissivity Measurements on Unencapsulated Solar Cells for Passive Thermal Control

Iñigo González de Arrieta, Telmo Echániz, Raquel Fuente, Gabriel A López

Angle-resolved direct emissivity measurements on unencapsulated solar cells for passive thermal control

Iñigo González de Arrieta, Telmo Echániz, Raquel Fuente, and Gabriel A. López

***Abstract*—The emissivity of two unencapsulated photovoltaic cells has been measured by a direct radiometric method, between 30 and 50 °C, and indirectly at room temperature. The advantages of the angle-resolved direct method for the determination of the emissivity of the bare cell, and the challenge of using direct measurements around room temperature, are discussed. This method allows calculating the total hemispherical emissivity by incorporating directional data, which are usually lacking. These data also reveal important differences between the infrared responses of both cells, despite the similarities in the more commonly reported normal spectra. These differences stem from the structure of the cells. A comparison to the integrating-sphere indirect method illustrates the improved accuracy of the emissivity values and their potential for evaluating the thermal performance of the cells and potential radiative cooling gains in select applications where the emissivity of the bare cell is not concealed by encapsulation. An estimation of the magnitude of this effect, obtained using a simplified heat-transfer model, is significantly less than 1% in absolute efficiency for realistic parameter values. More work is needed to quantify gains from encapsulated cells, which are expected to be even lower because of the higher emissivity of silica glass.**

***Index Terms*—infrared emissivity, thermal management, radiative cooling.**

I. Introduction

EMISSIVITY measurements on solar energy materials have attracted much attention over the years, especially in the case of absorbers for concentrated solar power [1]. The importance of this parameter for photovoltaic applications has traditionally been lower, given the reduced role of radiative heat transfer around room temperature. However, recent advances in radiative cooling have motivated an increase in the works devoted to this issue [2], [3], [4]. Temperature control in solar photovoltaic (PV) cells is crucial in order to achieve efficiencies as close as possible to the intrinsic Shockley-Queisser limit. Conversion efficiencies are typically linearly dependent on cell temperature, with temperature coefficients that can be as high as -0.5%/°C for crystalline silicon (c-Si) cells [5]. This leads to important efficiency losses with respect to the reported values at standard test conditions (STC, 25 °C, 1000 W/m^2, AM1.5), given that the real operation conditions can reach temperatures around 50 °C or even higher [6]. Due to the recent plateauing tendency of the intrinsic efficiencies of c-Si solar cells, thermal management is gaining attention as an efficiency-enhancing strategy [7].

Among the techniques available for thermal loss enhancement, radiative cooling has received particular attention due to its passive nature. This method involves making the emittance/absorptance of the material as high as possible in the mid-infrared atmospheric window (8-13 μm), and low in other ranges in order to reflect incident solar or atmospheric radiation. This cooling approach has been successfully implemented using a variety of methods and materials, even in daylight [4], [8]. However, one of the key premises of these methods is to reduce the amount of solar radiation absorbed by the material, a requirement which solar cells cannot meet. Thus, radiative cooling strategies can only be partially adopted in these materials, with spectral selectivity restricted to the infrared range. Studying the feasibility of this approach for selective absorbers on solar cells has been the stated goal of several studies with different cell architectures, with cooling figures greater than 10 °C often being reported [2], [3], [9], [10]. However, there are also authors who shed doubt on the capabilities of this strategy, stressing the need for accurate angle-resolved emissivity values and the effect of convective heat losses [11]. Other authors have also pointed out that the emissivities of bare cells, which are often used as the benchmark value, are often higher than those assumed [12]. Thus, estimating the gains from radiative cooling structures requires a careful consideration of the emissivities under play.

Not only standard solar cells can benefit from accurate emissivity characterizations. In addition to the standard single-junction cell architecture, other solar applications require thermal control (either for heat gain or loss). For example, radiative cooling is also being increasingly considered for concentrated photovoltaics [13] and thermophotovoltaics [14], [15], for which heat fluxes are much higher than for standard solar cells. In parallel to the research on high-emissivity structures for radiative cooling applications, there is also a need for low-emissivity solar cells for use in hybrid photovoltaic-thermal (PV-T) systems. This stems from the necessity to mitigate thermal losses to increase the outlet temperature of the fluid to the $40-60$ °C range [16], [17], [18]. Performance evaluation of more complex setups, like building-integrated photovoltaics, depends crucially on an accurate characterization of the emissivities of all components [19].

All the applications described above require knowledge

I. González de Arrieta and G. A. López are with the Department of Physics, University of the Basque Country UPV/EHU, E-48940 Leioa, Spain. E-mail: inigo.gonzalezdearrieta@ehu.eus

I. González de Arrieta is also with CNRS, CEMHTI UPR3079, Univ. Orléans, F-45071 Orléans, France.

T. Echániz and R. Fuente are with the Department of Applied Mathematics, University of the Basque Country UPV/EHU, E-48013 Bilbao, Spain.

Manuscript received XX; revised YY.

of the emissivity of photovoltaic materials in conditions for which measurements can be challenging. Radiometric emissivity measurements are typically divided into direct and indirect methods, both of which have been used for solar cell research. Traditional indirect methods rely on complementary techniques, such as reflectivity or ellipsometry measurements, which can be linked to the emissivity through optical relations. One of the most common indirect approaches concerns the use of room-temperature integrating spheres to measure the normal-hemispherical reflectivity [12], [18], [20]. This technique is well suited for near-to-mid-infrared characterization and is widely used at room temperature, but it suffers from poor accuracy at longer wavelengths ($\lambda > 10$ μm) and a lack of directionality. More complicated setups with directional and directional-hemispherical capabilities [21], [22], as well as ellipsometric techniques [18], have been devised to circumvent some of these limitations. On the contrary, direct methods, which rely on comparing the radiance emitted by the sample to that emitted by a blackbody, can compensate for these deficiencies, given a sufficiently accurate control of the temperatures [23], [24]. These methods facilitate the acquisition of directional data, as only sample rotation is necessary. The importance of accounting for the directionality of thermal emission is clear in solar thermal applications, as certain features which can lower or enhance the emissivity are only observable at oblique angles of incidence [25], [26]. Although total normal and hemispherical emissivities of materials are correlated [27], [28], important errors may occur when extrapolating one from the other. This is especially the case for multi-layer materials or complex surfaces, for which the common electromagnetic predictions for bulk materials do not hold. The main complication of these direct measurements is that all radiation sources (sample, background, detector) are of the same order of magnitude [23]. Other non-radiometric types of emissivity characterization involve calorimetric measurements based on heat flux measurements, which provide total hemispherical emissivity values directly [29], [30].

In this work, we report direct angular emissivity measurements at sample temperatures in the $30-50$ °C range, without any substantial alteration to the measurement method previously employed for high-temperature measurements [31]. This equipment has been used for characterization of solar-thermal collectors in vacuum and air [25], [26]. To our knowledge, this is the first time that a fully angle-resolved direct emissivity characterization has been undertaken for unencapsulated solar cells. Two types of monocrystalline silicon (mono-Si) cells have been selected, due to the complex dependence of thermal emission on the structure of solar cells [12].

II. Experimental details

Samples corresponding to two types of mono-Si solar cells have been investigated. Sample 1 is a 200 μm thick p-type aluminum back surface field cell (hereafter, BSF), with a textured surface and a SiN_x anti-reflective coating. Sample 2 is an interdigitated back contact n-type cell (hereafter, IBC) with a uniform anti-reflective coating and a thickness of 150 μm. In addition to the Si base, the current collectors, and the anti-reflective coating, two additional regions of highly doped silicon (n+ and p+) are present in the interfaces.

The emissivity measurements were made with the recently upgraded high-accuracy HAIRL emissometer of the University of the Basque Country [31]. This FTIR-based setup allows directional emissivity measurements in a controlled environment in a wide temperature range. The samples were measured under an argon atmosphere to avoid degradation and infrared absorption by atmospheric water and CO_2. The sample temperature was measured by two Type K thermocouples spot-welded to an ARMCO iron disk onto which the cell was glued using carbon paste. The radiation emitted by the sample enclosed in a colder blackbody environment is compared to two reference blackbody sources, a standard one at 800 °C and a room-temperature (21 °C) one. Crucially, the latter source is required to make an accurate calibration of the internal radiation of the emissometer [23]. To improve their signal-to-noise ratio, radiance measurements have been performed with the largest aperture possible without incurring in significant size-of-source effects. Finally, the integrated total emissivities have been calculated by a Monte Carlo procedure and extrapolation, by assuming that the observed spectral dependences of the emissivities continue outside the measured spectral range [31]. The amount of radiation contained at far-infrared wavelengths is of particular importance near room temperature, which makes this extrapolation procedure crucial for an accurate integration of the results.

The combined standard uncertainty of the emissivities for both cells at such temperatures increases monotonically from 5% at 5 μm to 11% at 23 μm [31]. This increase is related to the greater contribution of environmental radiation at longer wavelengths. The uncertainty increases rapidly at shorter wavelengths due to the very low signal emitted by the sample in that range and increased sensitivity to temperature measurement errors. Due to decreasing emissivity values with wavelength, the absolute uncertainties remain approximately constant throughout the measured spectral range.

An indirect method was also used for comparison purposes. The directional-hemispherical total reflectance (diffuse + specular components) was measured with an integrating sphere at an incident angle of 13°. This type of measurement is one of the most widely used for the characterization of solar coatings and solar cells at or near room temperature. This integrating sphere has a diameter of 75 mm and is equipped with a DLaTGS detector. The usual comparison measurement method has been used, by comparing the radiance reflected by the sample to that reflected by an Infragold® reference ($R_{ref} = 0.95$). The standard uncertainty is taken as the combination of uncertainties due to signal noise in the sample and reference reflectance measurements. It is small (2%) in the $\lambda < 10$ μm range, but increases quickly at longer wavelengths due to the low signal emitted by the source in that range. An additional source of systematic uncertainty beyond 15 μm is the increasingly non-Lambertian nature of the Infragold® coating [32].

III. Results and Discussion

A. Emissivity measurements

Normal spectral emissivity measurements were performed in both cells between 30 and 50 °C, as shown in Fig. 1. Even though the low signal makes for noisy measurements at short wavelengths, it was possible to obtain approximate values for the emissivity at wavelengths as short as 5 μm and temperatures as low as 30 °C. The low-temperature limit was conditioned by the nature of the measurement method, which diverges when the sample temperature approaches that of the sample enclosure [33]. The repeatability of these measurements suggests not only a very low temperature dependence, but also that the measurement is reliable and reproducible in this temperature limit. The most reliably measured range starts from about 8 μm, which is the one that accounts for most of the emitted radiation. Both cells show relatively high emissivities in the 8-14 μm atmospheric transparency range, with decreasing values at longer wavelengths. This supports the findings that the emissivities of unencapsulated silicon cells are not reproducible with data on bare silicon emissivities alone [12]. The source of high emissivity of solar cells compared with bare silicon is to be found on the relatively thin, but strongly absorbing, n+ and p+ doping layers. The use of bare silicon emissivity data, which is generally lower than 0.25, as representative of the emissivity of real unencapsulated solar cells (as in Refs. [2], [3]) is thus inaccurate.

Regarding the spectral dependence, both cells show decreasing emissivity with increasing wavelength, a behavior commonly found in metallic materials, although pure metals present much lower emissivity values [34]. This is consistent with the dominant optical absorption mechanism in highly doped silicon layers, which is free-electron based, but at much lower concentrations than in metals [12]. The emissivity of the BSF sample shows little temperature dependence in the $9-15$ μm range, with a somewhat more significant evolution at longer wavelengths, still barely outside the standard uncertainty range (depicted as a shaded area in Fig. 1). The temperature evolution below 9 μm shows no clear sign and is attributed to random variation. The spectra corresponding to the IBC cell, on the other hand, do not show any significant temperature evolution throughout the measured range. Nevertheless, these temperature-dependent measurements show that the results are reproducible within the standard uncertainty. This is to be expected, as this uncertainty is dominated by the systematic inaccuracy in temperature measurement, which is consistent for all measurements.

Besides, directional emissivity measurements were performed between 10° and 80° every 10° at a representative working temperature of 50 °C. Reported emission angles are defined relative to the macroscopically flat samples. Thus, they are defined without ambiguity, even if the texturing of solar cells is often of the order of magnitude of the wavelengths under study. This difference between local texture and macroscopic geometry is taken into account in well-known theoretical results, such as the Torrance-Sparrow model for the bidirectional reflectance distribution function (BRDF) [35], where the directional reflection is defined with respect to a coordinate system centered on the plane, but each of the individual micro-facets of the surface texture has a different orientation with respect to the plane. Fig. 2 depicts the results for both cells, which present different angular dependences. On the one hand, the BSF cell emissivity decreases with angle in a similar fashion throughout the entire measured spectrum. On the other hand, the IBC cell presents two different behaviors, depending on the spectral range. For wavelengths shorter than 10 μm, the IBC cell emissivity decreases continuously with angle, in a similar but less dramatic way to the BSF one. However, for longer wavelengths ($\lambda > 12$ μm), the emissivity increases up to 60-70° and then rapidly decreases at 80°. These behaviors can be appreciated in Fig. 3, where discrete emissivity values for three different wavelengths are displayed as a function of polar angle. The emissivity evolution seen in the BSF cell and in the IBC cell at shorter wavelengths is typically observed in dielectric materials while the IBC cell has a long-wavelength dependence similar to the one that metallic materials present, with an increase until high angles (around 70-80°) and a sudden drop-off. This could be due to the smaller thickness of the IBC cell, which means that the emission from the bottom metallic layer and back surface field (which is considered to be the most important factor [12])

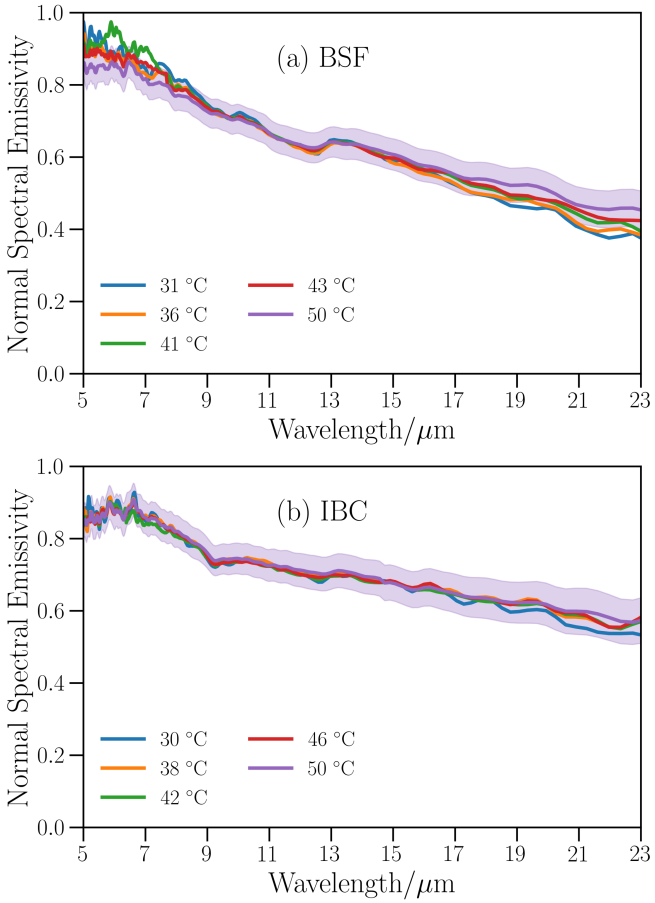

Fig. 1. Normal spectral emissivity of (a) the BSF cell and (b) the IBC cell as a function of temperature from approximately 30 to 50 °C. Shades correspond to the standard uncertainties (coverage factor $k = 1$) of the curves at 50 °C, which are very similar at all temperatures.

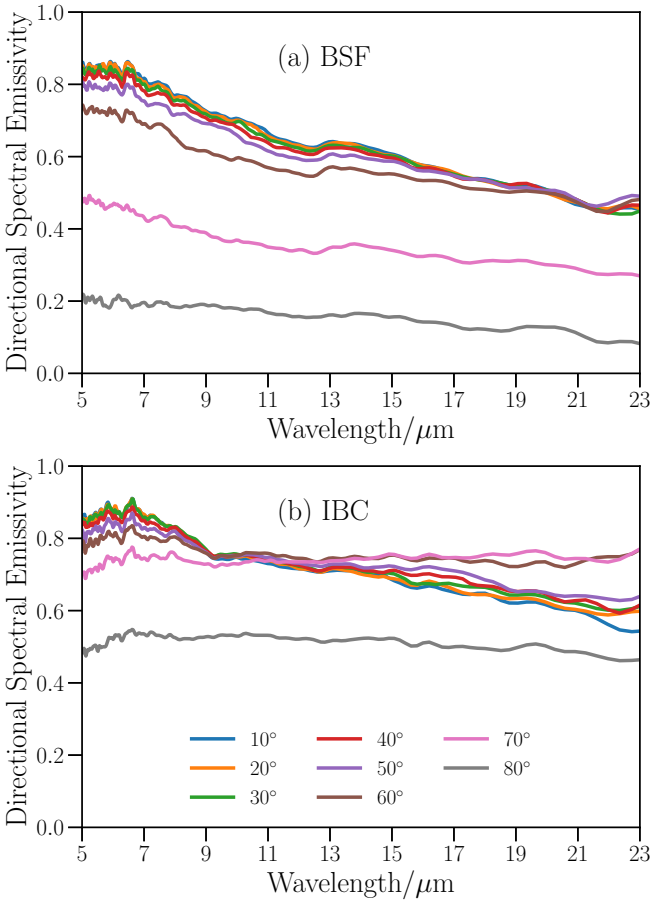

Fig. 2. Directional emissivity spectra at 50 °C for (a) the BSF cell and (b) the IBC cell. The code color in the legend applies to both subfigures.

is more pronounced. This may also be the reason why the off-normal emissivities remain much higher throughout the measured spectral range in this cell than in the BSF one. Nevertheless, it is well known that the emissivity of multilayer materials can present features that depend in a complex manner on wavelength and angle, which are not trivially linked to the optical properties of the main individual components [36]. More precise statements require an in-depth evaluation of the structure of each cell and the optical properties of each of its components, followed by numerical simulations. These topics are beyond the scope of the present work.

A comparison between the direct and indirect measurements, obtained with an integrating sphere, is shown in Fig. 4. A temperature of 50 °C has been chosen for the direct measurements in this comparison, as these curves are the most accurately measured, and no significant temperature dependence has been observed (Fig. 1). The results show relatively good agreement between both methods. This is an encouraging result since it validates the capabilities of direct emissivity measurements in this temperature range. In fact, the uncertainties obtained for the integrating sphere increase more rapidly for longer wavelengths ($\lambda > 18$ μm). Together with the possibility of measuring at working temperature and at different emission directions, the evidence suggests that direct

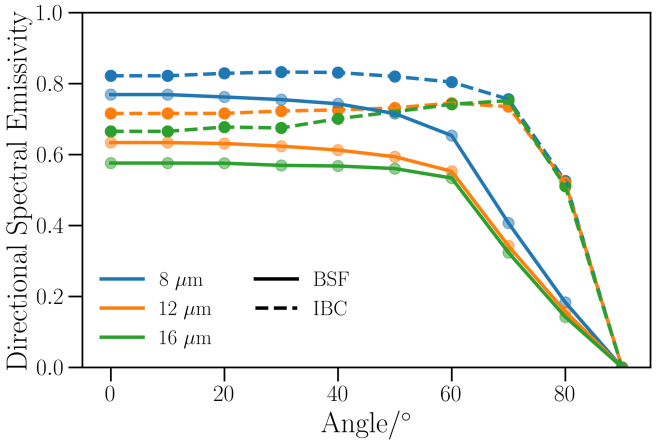

Fig. 3. Directional spectral emissivities at 50 °C for three discrete wavelengths (8, 12 and 16 μm) for the BSF cell (solid lines) and the IBC cell (dashed lines).

methods are an appropriate alternative for the characterization of high-emitting materials near room temperature.

Finally, the spectral emissivity curves obtained at 50 °C are integrated in wavelength and solid angle to obtain the total normal and total hemispherical emissivities (ε_N, ε_H). To integrate along the entire electromagnetic spectrum, data outside the reliably measured spectral range ($5-23$ μm) need to be extrapolated, as radiation outside that range accounts for a significant portion of the emitted radiation by a blackbody at temperatures around 50 °C. As the curves decrease monotonically, an upper and a lower limit of the emissivity values outside the measure range are taken [31]. These limits ensure an unbiased estimation of the uncertainty calculated for the total hemispherical emissivity values.

Due to the angular limitation of the indirect method, a comparison between total hemispherical emissivity values obtained by each method is not possible in principle. However, total hemispherical values may be estimated following the procedure described in Ref. [28]. An optical parameter $A = \varepsilon_H/\varepsilon_N$ is calculated from the electromagnetic theory, and tabulated as a function of the total normal emissivity. The correlation between the total normal and total hemispherical emissivities has been obtained from Ref. [34] for two limits: a perfect insulator (extinction index $k = 0$) and a good conductor ($k = n$, the real part of the refractive index). While the former approximation gives a factor of 0.96 for normal emissivities around 0.8, the latter gives a factor of 0.9. Because these cells show an intermediate behavior between these two situations, each approximation is given as a limit for the possible value of the total hemispherical emissivity. The results are shown in Table I for an assumed temperature of 50 °C. The temperature evolution is much lower than the experimental uncertainty, so it has been neglected. It can be seen that, although there is a certain agreement between both methods for determining the total normal emissivity, discrepancies arise when considering off-normal angles, due to the non-ideal nature of the material surface and its multi-layered structure. This renders approximations based on basic theoretical relations inaccurate.

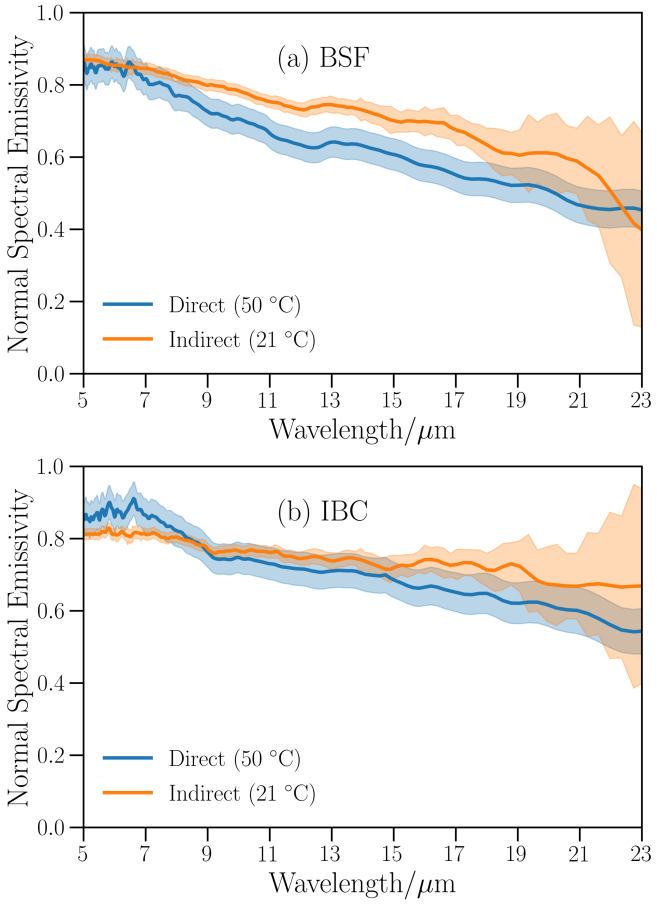

Fig. 4. Comparison of the normal spectral emissivity measured by the direct (50 °C) and indirect methods for (a) the BSF cell and (b) the IBC cell. Shaded regions correspond to the standard uncertainties ($k = 1$).

TABLE I
CALCULATED TOTAL NORMAL AND TOTAL HEMISPHERICAL EMISSIVITIES AND THEIR STANDARD UNCERTAINTIES ($k = 1$) FOR BOTH THE DIRECT AND INDIRECT METHODS, BOTH WEIGHTED BY BLACKBODY RADIATION CORRESPONDING TO A TEMPERATURE OF 50 °C. *: ESTIMATED USING THE NUMERICAL FACTORS 0.9 AND 0.96, AS DESCRIBED IN THE TEXT.

Sample		Direct	Indirect
BSF	ε_N	0.711 ± 0.047	0.772 ± 0.038
	ε_H	0.622 ± 0.048	$[0.695, 0.741]^*$
IBC	ε_N	0.789 ± 0.050	0.803 ± 0.044
	ε_H	0.795 ± 0.052	$[0.723, 0.771]^*$

Interestingly, the indirect estimations of ε_H show upward and downward bias for BSF and IBC, respectively. The role of off-normal angles is crucial, as they not only control most of the radiation emitted by the cell, but also most of the absorption of atmospheric radiation in radiative cooling applications [8].

It is worth noting that the emissivities of unencapsulated cells do not directly impact standard photovoltaic applications, given the opacity of the encapsulating glass in the mid-infrared. However, these reference values can still be useful for more complex geometries, such as photovoltaic-thermal [17] or building-integrated systems [19], where the direct emission from the silicon cell must be taken into account. Moreover, these measurements serve to illustrate the usefulness of the direct method for the characterization of materials for near-room-temperature applications. In the following section, a brief comment on how to use these values to estimate potential radiative cooling gains is exposed.

B. Radiative cooling potential

The measured emissivities and absorptances of the cells can be used to estimate their heat balance in operation, to determine reference values of temperature and efficiency which radiative cooling approaches can be compared to. It has been assumed in the literature that the unencapsulated cell sets the standard for the hottest configuration, due to the low emissivity of bare silicon [2], [3]. Nevertheless, the emissivity of unencapsulated cells has been shown to be much larger than what is conventionally assumed (due to the influence of the highly doped layers [12]). Therefore, the availability of directional values for the emissivities of the cells motivates an estimation of the potential of radiative cooling for these materials.

Due to the large thermal conductivities of silicon and aluminum and the low thicknesses of the unencapsulated cells, an isothermal approximation can be used. Under such approximation, the heat balance can be approximated by:

$$P_S + P_{atm} = P_{el}(T) + P_{rad}(T) + P_{con}(T) \tag{1}$$

where T is the isothermal cell temperature for which the above balance holds, and each power term P (solar, atmospherical, electrical, radiative and conductive-convective) is defined as following:

$$P_S = \int (1 - R(\lambda, 0°)) I_S(\lambda) d\lambda = \alpha_S I_S \tag{2}$$

$$P_{atm} = \int d\Omega \cos\theta \int \varepsilon(\lambda, \theta)(1 - \tau(\lambda))^{1/\cos\theta} L_b(\lambda, T) d\lambda \tag{3}$$

$$P_{rad} = \int d\Omega \cos\theta \int \varepsilon(\lambda, \theta) L_b(\lambda, T) d\lambda = \varepsilon_H \sigma T^4 \tag{4}$$

$$P_{con} = h(T - T_0) \tag{5}$$

where I_S is the solar irradiance, $R(\lambda, 0°)$ is the normal-hemispherical reflectivity measured using a UV-Vis-NIR spectrophotometer, $\varepsilon(\lambda, \theta)$ is the directional emissivity determined using the FTIR-based HAIRL radiometer, $L_b(\lambda, T)$ is the spectral radiance of a blackbody, and $\tau(\lambda)$ is the normal transmittance of the atmosphere, as reported in the literature [37], [38]; while h corresponds to the heat transfer coefficient of the entire cell, including both the bottom and top surfaces ($h = h_1 + h_2$).

The electrical power, corresponding to the useful absorbed solar energy, is sometimes estimated from the Shockley-Queisser limit [9], [39], [15]. In this case, this term is computed from the efficiency and temperature coefficients of the cells:

$$P_{el}(T) = \eta(T) I_S = \eta_{STC}[1 - \beta(T - 298.15)] I_S \tag{6}$$

where η is the solar cell efficiency, STC denotes Standard Testing Conditions, β stands for the temperature coefficient, and T is the absolute temperature.

The directional spectral emissivity of the atmosphere can be obtained from its tabulated transmittance in the zenith direction [8]. The Cerro Pachon spectrum corresponding to the standard AM1.5 air mass and a water column height of 10.0 mm have been assumed as representative [37], [38]. This water vapor content, which is the highest humidity value available in the reference, is representative of relatively dry areas [40] and similar to the one assumed in the AM1.5 solar irradiance standard (14.2 mm). For wetter areas, the secondary transmission window (16-26 μm) will disappear and the emissivity in the main 8-13 μm transparency window will also increase, thus significantly affecting radiative cooling potentials [41]. These situations are neglected in this work for simplicity.

The equilibrium temperatures are obtained by finding the root of Eq. 1 using the secant method, for each set of independent variables and a starting temperature of 30 °C. More sophisticated modeling of these features can be obtained by several methods, namely those based on the radiative-transfer equation, electromagnetic simulations, and multiphysical approaches [2], [42]. Nevertheless, simple heat-transfer models can be useful approximations to understand the effects of solar cell emissivity.

The equilibrium temperatures are shown in Fig. 5a, while the absolute gains in temperature and efficiency are represented in Fig. 5b. A solar irradiance value of 800 W/m^2 and an ambient temperature of 27 °C were chosen, following Ref. [2]. All optical and electrical parameters aside from the emissivity (solar absorptance, conversion efficiency, and temperature coefficient) are kept constant at realistic values for all three curves ($\alpha_S = 0.92$, $\eta = 20.0\%$, $\beta = -0.04\,\%/°\text{C}$). This is purposefully made to avoid comparisons between the performances of each cells and to illustrate the effect of the emissivity on cooling. As expected, the sample with the lower emissivity (BSF) benefited the most from the addition of a perfect emitter in terms of both temperature reduction and efficiency increase. Very significant radiative cooling figures can be obtained for both cells, but only in the cases of extremely low non-radiative heat dissipation. For heat-transfer coefficient values below 10 W/m^2°C, the BSF cell can reach radiative cooling values greater than 10 °C and absolute efficiency gains reaching 1%, consistent with several claims based on numerical simulations and the experiment in Ref. [3], which reaches a maximum cooling value of 13 °C. It must be noted that the emissivity of the bare cell used in the latter work only simulates a real solar cell, and thus its emissivity is much lower than the ones in our study. This is the reason why such large cooling values are only found in our model for low heat-transfer coefficient values, corresponding to conditions that are unlikely to be found in terrestrial environments. Even considering an already modest value of $h = 10$ W/m^2°C, the cooling effect for the BSF architecture when coated with a perfect infrared emitter is 6.4 °C, and only 3.8 °C for the IBC cell. These values translate into estimated potential absolute efficiency gains of 0.51% and 0.31%, respectively. These constitute marginal improvements, particularly considering that for, the vast majority of practical applications, the cells are encapsulated by silicate glasses, with much higher emissivities in the mid-infrared. Therefore, such kinds of analysis starting from bare-cell emissivities lead intrinsically to overestimated cooling figures. However, for special cases where unencapsulated solar cells are used and non-radiative heat losses are limited, this framework provides a potential efficiency-increasing route.

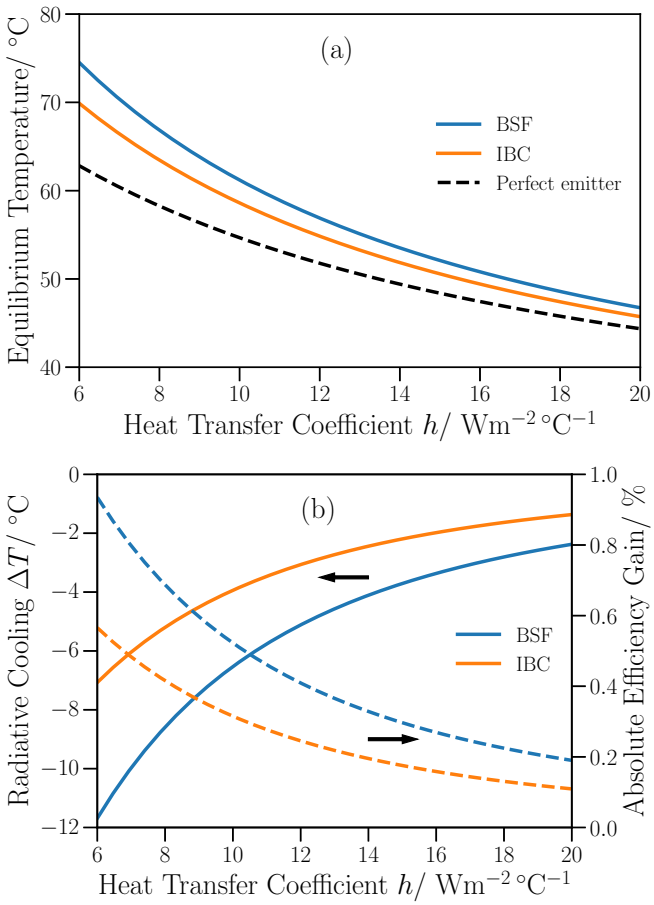

Fig. 5. (a) Estimation of the equilibrium temperatures of the bare cells and those coated with a perfect diffuse emitter in the infrared. Only the emissivity of the cells is varied in the simulations, in order to isolate its effect. (b) Absolute radiative cooling (left, solid lines) and the associated efficiency gain (right, dashed lines). Solar irradiance and environment temperature are fixed at representative values ($I_S = 800$ W/m^2, $T_0 = 27$ °C), while the strength of conductive-convective heat transfer mechanisms is allowed to vary.

IV. Conclusions

This work reports on a comparison and validation of direct emissivity measurements for the study of the radiative properties of solar photovoltaic cells. The emissivities of both unencapsulated cells are much higher than that of bare silicon, because of the presence of highly doped regions. Even though their spectral dependence in the normal direction is similar, important differences are observed at higher angles of emission. The direct measurement method, which is often considered too unreliable for these applications because of their low temperatures, is shown to be accurate down to temperatures

very close to those of the enclosure, the fundamental limit of this method. These measurements are also intrinsically useful, as they provide temperature-dependent and angle-resolved data for all kinds of surfaces, which allows calculating their total hemispherical emissivity. They can also provide more in-depth analyses of the infrared properties of these materials, and how the different components affect the overall emission. This information is relevant for thermal modeling of select photovoltaic applications in which the unencapsulated surface is responsible for thermal emission, as well as to establish more reliable benchmarks for estimating potential radiative cooling gains. A simplified heat-transfer model based on these data allowed estimating the potential degree of radiative cooling of these cells, which was small but potentially important in certain applications. To be of greater industry relevance, future work should focus on the effects of encapsulation, given its potential of concealing the emissivity of the bare cells, as well as the long-term reliability of the cells and their optical properties.

ACKNOWLEDGMENT

The authors acknowledge funding from the Basque Government (PIBA-2021-1-0022, IT1714-22). I. González de Arrieta thanks the Basque Government for its support through a postdoctoral fellowship (POS-2021-2-0022).

REFERENCES

[1] T. Echániz, I. Setién-Fernández, R. B. Pérez-Sáez, C. Prieto, R. E. Galindo, and M. J. Tello, "Importance of the spectral emissivity measurements at working temperature to determine the efficiency of a solar selective coating," *Sol. Energ. Mat. Sol. C.*, vol. 140, pp. 249–252, Sep. 2015.

[2] L. Zhu, A. Raman, K. X. Wang, M. A. Anoma, and S. Fan, "Radiative cooling of solar cells," *Optica*, vol. 1, no. 1, pp. 32–38, Jul. 2014.

[3] L. Zhu, A. P. Raman, and S. Fan, "Radiative cooling of solar absorbers using a visibly transparent photonic crystal thermal blackbody," *P. Natl. Acad. Sci. USA*, vol. 112, no. 40, pp. 12 282–12 287, Sep. 2015.

[4] A. P. Raman, M. A. Anoma, L. Zhu, E. Rephaeli, and S. Fan, "Passive radiative cooling below ambient air temperature under direct sunlight," *Nature*, vol. 515, no. 7528, p. 540, Nov. 2014.

[5] O. Dupr, R. Vaillon, and M. Green, "Physics of the temperature coefficients of solar cells," *Sol. Energ. Mat. Sol. C.*, vol. 140, pp. 92–100, Sep. 2015.

[6] M. Koehl, M. Heck, S. Wiesmeier, and J. Wirth, "Modeling of the nominal operating cell temperature based on outdoor weathering," *Sol. Energ. Mat. Sol. C.*, vol. 95, no. 7, pp. 1638–1646, Jul. 2011.

[7] R. Vaillon, O. Dupré, R. B. Cal, and M. Calaf, "Pathways for mitigating thermal losses in solar photovoltaics," *Sci. Rep.*, vol. 8, no. 1, p. 13163, Sep. 2018.

[8] E. Rephaeli, A. Raman, and S. Fan, "Ultrabroadband photonic structures to achieve high-performance daytime radiative cooling," *Nano Lett.*, vol. 13, no. 4, pp. 1457–1461, Mar. 2013.

[9] T. S. Safi and J. N. Munday, "Improving photovoltaic performance through radiative cooling in both terrestrial and extraterrestrial environments," *Opt. Express*, vol. 23, no. 19, pp. A1120–A1128, Sep. 2015.

[10] J. N. Munday and T. Safi, "Radiative cooling of a GaAs solar cell to improve power conversion efficiency," in *IEEE 43rd Photovoltaic Specialists Conference (PVSC)*, Nov. 2016, pp. 1125–1127.

[11] A. Gentle and G. Smith, "Is enhanced radiative cooling of solar cell modules worth pursuing?" *Sol. Energ. Mat. Sol. C.*, vol. 150, pp. 39–42, Jun. 2016.

[12] A. Riverola, A. Mellor, D. A. Alvarez, L. F. Llin, I. Guarracino, C. Markides, D. Paul, D. Chemisana, and N. Ekins-Daukes, "Mid-infrared emissivity of crystalline silicon solar cells," *Sol. Energ. Mat. Sol. C.*, vol. 174, pp. 607–615, Jan. 2018.

[13] Z. Zhou, Z. Wang, and P. Bermel, "Radiative cooling for low-bandgap photovoltaics under concentrated sunlight," *Opt. Express*, vol. 27, no. 8, pp. A404–A418, Apr. 2019.

[14] E. Blandre, R. Vaillon, and J. Drévillon, "New insights into the thermal behavior and management of thermophotovoltaic systems," *Opt. Express*, vol. 27, no. 25, pp. 36 340–36 349, Dec. 2019.

[15] Z. Zhou, X. Sun, and P. Bermel, "Radiative cooling for thermophotovoltaic systems," in *Infrared Remote Sensing and Instrumentation XXIV*, M. Strojnik, Ed., vol. 9973, International Society for Optics and Photonics. SPIE, Sep. 2016, pp. 53–60.

[16] M. Lämmle, T. Kroyer, S. Fortuin, M. Wiese, and M. Hermann, "Development and modelling of highly-efficient PVT collectors with low-emissivity coatings," *Sol. Energy*, vol. 130, pp. 161–173, Jun. 2016.

[17] A. Mellor, D. A. Alvarez, I. Guarracino, A. Ramos, A. R. Lacasta, L. F. Llin, A. J. Murrell, D. J. Paul, D. Chemisana, C. N. Markides, and N. J. Ekins-Daukes, "Roadmap for the next-generation of hybrid photovoltaic-thermal solar energy collectors," *Sol. Energy*, vol. 174, pp. 386–398, Nov. 2018.

[18] D. Alonso-lvarez, A. Augusto, P. Pearce, L. F. Llin, A. Mellor, S. Bowden, D. Paul, and N. Ekins-Daukes, "Thermal emissivity of silicon heterojunction solar cells," *Sol. Energ. Mat. Sol. C.*, vol. 201, p. 110051, Oct. 2019.

[19] L. Granados, S. Huang, D. R. McKenzie, and A. W. Y. Ho-Baillie, "The importance of total hemispherical emittance in evaluating performance of building-integrated silicon and perovskite solar cells in insulated glazings," *Appl. Energy*, vol. 276, p. 115490, Oct. 2020.

[20] A. Roos, "Use of an integrating sphere in solar energy research," *Sol. Energ. Mat. Sol. C.*, vol. 30, no. 1, pp. 77–94, Jun. 1993.

[21] I. Subedi, T. J. Silverman, M. G. Deceglie, and N. J. Podraza, "Emissivity of solar cell cover glass calculated from infrared reflectance measurements," *Sol. Energ. Mat. Sol. C.*, vol. 190, pp. 98–102, Feb. 2019.

[22] A. Parretta, A. Sarno, P. Tortora, H. Yakubu, P. Maddalena, J. Zhao, and A. Wang, "Angle-dependent reflectance measurements on photovoltaic materials and solar cells," *Opt. Commun.*, vol. 172, no. 1-6, pp. 139–151, Dec. 1999.

[23] Y. Xiao, A. Shahsafi, C. Wan, P. J. Roney, G. Joe, Z. Yu, J. Salman, and M. A. Kats, "Measuring thermal emission near room temperature using Fourier-transform infrared spectroscopy," *Phys. Rev. Appl.*, vol. 11, no. 1, p. 014026, Jan. 2019.

[24] D. Labuhn and S. Kabelac, "The spectral directional emissivity of photovoltaic surfaces," *Int. J. Thermophys.*, vol. 22, no. 5, pp. 1577–1592, Sep. 2001.

[25] A. Dan, B. Basu, T. Echániz, I. González de Arrieta, G. López, and H. Barshilia, "Effects of environmental and operational variability on the spectrally selective properties of W/WAlN/WAlON/Al_2O_3-based solar absorber coating," *Sol. Energ. Mat. Sol. C.*, vol. 185, pp. 342–350, Oct. 2018.

[26] I. González de Arrieta, T. Echániz, R. Fuente, E. Rubin, R. Chen, J. M. Igartua, M. J. Tello, and G. A. López, "Infrared emissivity of copper-alloyed spinel black coatings for concentrated solar power systems," *Sol. Energ. Mat. Sol. C.*, vol. 200, p. 109961, Sep. 2019.

[27] M. Rubin, D. Arasteh, and J. Hartmann, "A correlation between normal and hemispherical emissivity of low-emissivity coatings on glass," *Int. Commun. Heat Mass*, vol. 14, no. 5, pp. 561–565, Sep. 1987.

[28] J.-P. Monchau, J. Hameury, P. Ausset, B. Hay, L. Ibos, and Y. Candau, "Comparative study of radiometric and calorimetric methods for total hemispherical emissivity measurements," *Heat Mass Transfer*, vol. 54, no. 5, pp. 1415–1425, May 2018.

[29] B. G. Lohan, M. Amara, A. Kaminski-Cachopo, and M. Lemiti, "Innovative experimental setup for thermal and electrical characterization of silicon solar cells under controlled environmental conditions," *Sol. Energ. Mat. Sol. C.*, vol. 185, pp. 300–306, Oct. 2018.

[30] L. Granados, N. Takamure, J. Bing, S. Huang, H. Merhvarz, D. R. McKenzie, and A. Ho-Baillie, "Direct determination of total hemispherical emittance of perovskite and silicon solar cells," *Cell Rep. Phys. Sci.*, vol. 1, no. 1, p. 100008, Jan. 2020.

[31] I. González de Arrieta, T. Echániz, R. Fuente, J. M. Campillo-Robles, J. M. Igartua, and G. A. López, "Updated measurement method and uncertainty budget for direct emissivity measurements at the University of the Basque Country," *Metrologia*, vol. 57, p. 045002, Jul. 2020.

[32] L. M. Hanssen and K. A. Snail, "Integrating spheres for mid-and near-infrared reflection spectroscopy," in *Handbook of Vibrational Spectroscopy*, P. Griffiths and J. M. Chalmers, Eds. John Wiley & Sons, Ltd New York, 2006, pp. 1175–1192.

[33] R. B. Pérez-Sáez, L. del Campo, and M. J. Tello, "Analysis of the accuracy of methods for the direct measurement of emissivity," *Int. J. Thermophys.*, vol. 29, no. 3, pp. 1141–1155, Mar. 2008.

[34] J. R. Howell, M. P. Menguc, and R. Siegel, *Thermal Radiation Heat Transfer*, 6th ed. Boca Raton: CRC Press, 2015.

[35] K. E. Torrance and E. M. Sparrow, "Theory for off-specular reflection from roughened surfaces," *J. Opt. Soc. Am.*, vol. 57, no. 9, pp. 1105–1114, Sep. 1967.
[36] A. Dan, M. Sainz-Menchón, J. Gabirondo-López, T. Echániz, R. Fuente, G. A. López, and H. C. Barshilia, "Emissivity measurements of W/TiAlN/TiAlSiN/TiAlSiON/TiAlSiO-based multilayer spectrally selective absorbers at high temperature," *Sol. Energy*, vol. 252, pp. 403–412, Mar. 2023.
[37] S. D. Lord, "NASA Technical Memorandum 103957 - A new software tool for computing Earth's atmospheric transmission of near- and far-infrared radiation," 1992.
[38] Gemini Observatory, "IR Transmission Spectra," retrieved Nov 15, 2019. [Online]. Available: https://www.gemini.edu/?q=node/10789
[39] Y.-W. Lin, E. L. Schlenker, Z. Zhiguang, and P. Bermel, "Radcool: a web-enabled simulation tool for radiative cooling," 2017. [Online]. Available: https://nanohub.org/resources/26902
[40] B. Chen and Z. Liu, "Global water vapor variability and trend from the latest 36-year (1979 to 2014) data of ECMWF and NCEP reanalyses, radiosonde, GPS, and microwave satellite," *J. Geophys. Res.-Atmos.*, vol. 121, no. 19, pp. 11,442–11,462, Oct. 2016.
[41] M. Li and C. F. M. Coimbra, "On the effective spectral emissivity of clear skies and the radiative cooling potential of selectively designed materials," *Int. J. Heat Mass Tran.*, vol. 135, pp. 1053–1062, Jun. 2019.
[42] L. Weiss, M. Amara, and C. Ménézo, "Impact of radiative-heat transfer on photovoltaic module temperature," *Prog. Photovoltaics*, vol. 24, no. 1, pp. 12–27, Jan. 2016.

Assistant Professor Iñigo González de Arrieta holds a PhD degree in Physics (University of the Basque Country, 2020). After working as a post-doctoral researcher at CNRS Orléans (France), he obtained an Assistant Professorship at the University of the Basque Country in Leioa (Spain). His work, which is reflected in 16 articles in JCR-indexed journals, is focused on infrared spectroscopy and the optical properties of materials, with special attention to radiative heat transfer. Dr. González de Arrieta is a member of the European Optical Society and the Coblentz Society. He has performed reviewing duties for 13 indexed journals, including two IOP Outstanding Reviewer Awards in 2020 and 2021.

Associate Professor Telmo Echániz obtained his Bachelor's Degree in Physics in the University of the Basque Country in 2011, where he also obtained his Material Physics and Technology Master's Degree in 2012 and the Ph.D. Degree in the Condensed Matter Physics Department in 2016, where he specialized in the study of spectral emissivity in metallic materials and materials for solar applications. In 2017 he became an Asssistant Professor in the Applied Mathematics Department in the University of the Basque Country (Bilbao, Spain). He is an Associate Professor in the same department since 2023. He currently has more than 20 indexed and peer-reviewed articles (h=12) and is a reviewer of 10 JCR journals.

Assoc. Prof. Raquel Fuente received her degree in Physics in 2008 and her Ph.D. in Engineering in 2012, recognized with the extraordinary doctorate award, from the University of the Basque Country. Also, she worked in laboratories in Belgium (KU Leuven) and Canada (CADIFT, UofT), doing research in all cases in projects, public and industrial, related to the thermal and optical characterization of materials by infrared radiometry. Afterwards, she joined a technology center, IK4-Lortek, where she was responsible for the research line in non-destructive tests by infrared thermography. She is currently an Associate Professor at the Faculty of Engineering of Bilbao (University of the Basque Country) and a researcher in the Thermophysical Properties of Materials group. She works in the spectral radiometric characterization of the thermal and optical properties of materials, where she is focused on the most applied research field, in particular on solar energy and high-temperature industrial cases. She is a Principal Investigator in several projects, author of numerous articles and contributions to conferences, and usual reviewer for JCR journals.

Assoc. Prof. Gabriel A. López after getting a degree in Chemical Engineering at the National University of Comahue (Argentina) he got his Ph.D. on Materials Science at the Max Planck Institute for Metals Research in Stuttgart (Germany). Then, through a Marie Curie Fellowship, he moved to the University of the Basque Country UPV/EHU (Bilbao, Spain) where he broadened his expertise on electron microscopy and physical metallurgy. Since July 2016 he is Assoc. Professor at the UPV/EHU and in charge of the Research Group on Thermophysical Properties of Materials. He is also Vice-dean for Students Affairs of the Faculty of Science and Technology of the UPV/EHU. He has published more than 60 indexed articles (h=16), participated in multiple research projects, given several invited talks in international conferences, is member of the Editorial Board of a JCR journal and is reviewer for various journals.